# OVERVIEW OF ATLAS HEAVY FLAVOR MEASUREMENTS*

Sally Seidel

on behalf of the ATLAS Collaboration

Department of Physics and Astronomy, University of New Mexico
Albuquerque, NM 87131, USA

*(Received April 20, 2018)*

The ATLAS Experiment presents four recent measurements in the field of $B$-physics using data recorded at the center-of-mass energy of 8 TeV at the LHC. All are compared to contemporary models. These measurements involve differential cross sections for $b$-hadron pair production; prompt $J/\psi$ pair production differential cross sections; differential production cross sections for $\psi(2S)$ and $X(3872)$, both observed in decays to $J/\psi\pi^+\pi^-$; and an angular analysis of $B^0_d \to K^*\mu^+\mu^-$ decays.

DOI:10.5506/APhysPolB.49.1359

## 1. Introduction

The four most recent results in $B$-physics by the ATLAS Experiment [1] are presented. All four use LHC proton–proton collision data collected at center-of-mass energy 8 TeV, and all were released in 2017.

## 2. The $b$-hadron pair production cross section

The production of $b$- and $c$-quarks (hereafter called heavy flavor) in proton–proton collisions provides a fruitful testing ground for the predictions of quantum chromodynamics (QCD). The mass of the $b$-quark introduces a scale, and the factorization of QCD calculations into parton distribution functions, hard matrix element, and softer parton shower components allows the mass to be introduced at different stages. Furthermore, there are several possible schemes for the inclusion of the heavy quark masses at the various stages. The optimal settings must be determined by comparison to

* Presented at the Cracow Epiphany Conference on Advances in Heavy Flavour Physics, Kraków, Poland, January 9–12, 2018.

data. Previous measurements have highlighted disagreements both between different theoretical predictions and between those predictions and the data. The realm of small angle $b\bar{b}$ pair production is particularly sensitive to the details of the calculations but remains only loosely constrained by data. Searches for Higgs bosons produced in association with a vector boson and decaying to a $b\bar{b}$ pair rely extensively on the modeling of the background arising from QCD production of $b\bar{b}$ pairs in association with vector bosons.

Motivated by these facts, a measurement [2] has been made of the production of two $b$ hadrons, where one $b$-hadron decays to $J/\psi(\to \mu^+\mu^-) + X$ and the other to $\mu + Y$, resulting in three muons in the final state. The signal definition includes $J/\psi$ mesons produced via feed-down from excited charmonium states as well as muons produced in semileptonic cascade decays. To probe $b$-hadron production, several differential cross sections are measured, based on the kinematics of the $J/\psi$ (reconstructed from two muons) and the third muon. The variables considered are:

— the azimuthal separation $\Delta\phi(J/\psi, \mu)$ between the $J/\psi$ and the third muon;

— the transverse momentum of the three-muon system, $p_{\mathrm{T}}(J/\psi, \mu)$;

— the separation between the $J/\psi$ and the third muon in the azimuth-rapidity plane, $\Delta R(J/\psi, \mu)$;

— the separation in rapidity $\Delta y(J/\psi, \mu)$ between the $J/\psi$ and the third muon;

— the magnitude of the average rapidity of the $J/\psi$ and the third muon, $y_{\mathrm{boost}}$;

— the mass of the three-muon system, $m(J/\psi, \mu)$;

— the ratio of the transverse momentum of the three-muon system to the invariant mass of the three-muon system, $p_{\mathrm{T}}/m$, and its inverse, $m/p_{\mathrm{T}}$.

The differential cross sections are measured and compared to predictions from several Monte Carlo generators.

Events are selected using a dimuon trigger where the muons are required to have opposite charge, be consistent with originating at the same production vertex, have $p_{\mathrm{T}}(\mu) > 4$ GeV and pseudo-rapidity $|\eta(\mu)| < 2.4$, and satisfy $2.5 < m(\mu^+\mu^-) < 4.3$ GeV. The integrated luminosity of the data set is 11.4 fb$^{-1}$. Following selection of the primary vertex (defined as the vertex formed from at least two tracks, each with $p_{\mathrm{T}} > 400$ MeV, that has the largest summed track $p_{\mathrm{T}}^2$ in the event), muon candidates are formed,

and $J/\psi$ candidates are reconstructed from them. The third muon is then selected as the highest-$p_{\mathrm{T}}$ muon not used in the $J/\psi$ candidate reconstruction. To extract the $J/\psi$ mesons resulting from the decay of a $b$-hadron, a simultaneous fit is performed upon the distributions of dimuon mass and the pseudo-proper decay time $\tau$, defined as

$$\tau = L_{xy}\, m(J/\psi_{\mathrm{PDG}})/p_{\mathrm{T}}\left(\mu^{+}\mu^{-}\right) ,$$

where $L_{xy}$ is the signed transverse distance between the primary vertex and the dimuon vertex

$$L_{xy} = \frac{\vec{L}\cdot\vec{p}_{\mathrm{T}}}{p_{\mathrm{T}}} .$$

Because $J/\psi$ mesons produced by most $b$-hadron decays are non-prompt, a selection $\tau > 0.25$ mm$/c$ is applied.

Following the addition of the third muon, the yield of signal events relative to background is further improved using a simultaneous fit to the transverse impact parameter significance and the output of a boosted decision tree trained to separate signal muons from misreconstructed muons. The transverse impact parameter significance is defined as $S_{d_0} \equiv d_0/\sigma_{d_0}$, where $d_0$ is the signed distance of closest approach of the track to the primary vertex point in the $r$–$\phi$ projection and $\sigma_{d_0}$ is the unsigned uncertainty on the reconstructed $d_0$. Some remaining irreducible sources of background are then subtracted from the fitted yields. Corrections for the effects of the selection on $\tau$ and for the effects of detector resolution are applied, and the analysis is repeated for every kinematic bin for each differential cross section, resulting in the cross section in that bin.

The total measured cross section in the fiducial region (see [2], Section 3.3) is

$$\sigma\left(B\left(\rightarrow J/\psi\left[\rightarrow \mu^{+}\mu^{-}\right]+X\right)B(\rightarrow \mu+X)\right) = 17.7\pm0.1(\mathrm{stat.})\pm2.0(\mathrm{syst.})\mathrm{nb}\,.$$

The data are compared to predictions by various simulations including that for inclusive $b$-hadron pairs taken from Pythia8.186. These explore several options for the $g \rightarrow b\bar{b}$ splitting kernel as this process dominates small-angle $b$-hadron production. The settings explore whether to use the relative $p_{\mathrm{T}}$ or mass of the splitting to set the scale when determining the value of $\alpha_{\mathrm{s}}$ to use in that splitting. It is found that, in general, Pythia8 does not reproduce the shape of the angular distributions in data within uncertainties, and the $p_{\mathrm{T}}$-based scale splitting kernels generally give a better description of the low $\Delta R(J/\psi, \mu)$ region.

The comparisons are then extended to predictions using Herwig++, MadGraph5_aMC@NLOv2.2.2 interfaced to the Pythia8.186 parton shower model, and Sherpa2.1.1. Options with 5-flavor and 4-flavor schemes are compared. The comparisons indicate that: (1) agreement with data is slightly better for Herwig++ than Pythia8 in the $\Delta R(J/\psi, \mu)$ distribution; (2) the 4-flavor prediction by MadGraph+Pythia8 is generally closer in shape to the data than the 5-flavor prediction; (3) in $\Delta y(J/\psi, \mu)$, the MadGraph+Pythia and Sherpa predictions provide a good description of the data; (4) in $y_{\text{boost}}$, all models are comparable; (5) the 5-flavor MadGraph+Pythia8 prediction lies closer to data than the 4-flavor one in the low mass distribution; and (6) at high values of $p_{\text{T}}/m$, the 4-flavor prediction describes the data better than the 5-flavor prediction. Considering all distributions, the 4-flavor MadGraph+Pythia8 prediction provides the best description of the data overall, the predictions of Pythia8 and Herwig++ are comparable, and of the Pythia8 options considered, the $p_{\text{T}}$-based splitting kernel gives the best agreement with data. Figure 1 compares the various predictions to the measured normalized differential cross section in $p_{\text{T}}/m$.

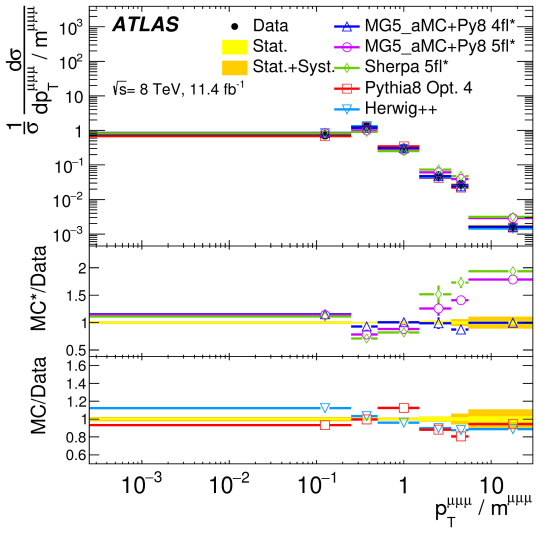


Fig. 1. The measured normalized differential cross section as a function of $p_{\text{T}}/m$. Comparisons are made with predictions of Pythia8 and Herwig++. MadGraph5_aMC@NLO+Pythia8 and Sherpa predictions are also compared having been corrected from the two-$b$-hadron production to the three-muon final state via transfer functions (indicated with $^*$). The Pythia8 "Opt. 4" gluon splitting parameter settings use a splitting kernel $z^2 + (1-z)^2 + 8r_q z(1-z)$, normalized so that the $z$-integrated rate is $(\beta/3)(1 + r/2)$, and with an additional suppression factor $(1 - m_{qq}^2/m_{\text{dipole}}^2)^3$, which reduces the rate of high-mass $q\bar{q}$ pairs.

### 3. The prompt $J/\psi$ pair production cross section

The production of two prompt $J/\psi$ mesons, produced centrally in the ATLAS detector, is studied [3]. The requirement of promptness translates to a demand that their point of production be consistent with the primary vertex in the event, indicating that they not be the products of the decay of long-lived hadrons. Differential cross sections are measured for this process as a function of the transverse momentum $p_{\mathrm{T}}$ of the lower-$p_{\mathrm{T}}$ $J/\psi$ meson, the di-$J/\psi$ $p_{\mathrm{T}}$ and mass, the difference in rapidity between the two $J/\psi$ mesons, and the azimuthal angle between them. Characterization of kinematic correlations between the two $J/\psi$ mesons is used to extract the fraction of prompt pair events that arise due to double parton scattering (DPS). This is the first such measurement at the center-of-mass energy of 8 TeV, and it probes a different kinematical range from previous such measurements at 1.96 TeV and 7 TeV. At the LHC energies, $J/\psi$ meson production is dominated by gluon–gluon interactions, so the DPS cross section is sensitive to the spatial distribution of gluons in the proton. An Ansatz for defining the DPS cross section in terms of the production cross sections of the two final states, the fraction $f_{\mathrm{DPS}}$ of prompt–prompt di-$J/\psi$ events that are due to DPS, and an effective cross section $\sigma_{\mathrm{eff}}$ is

$$\sigma_{\mathrm{eff}} = \frac{1}{2}\frac{\sigma^2_{J/\psi}}{\sigma^{J/\psi,J/\psi}_{\mathrm{DPS}}} = \frac{1}{2}\frac{\sigma^2_{J/\psi}}{f_{\mathrm{DPS}}\,\sigma_{J/\psi J/\psi}}\,.$$

Testing possible correlations of non-perturbative origin between the partons in DPS events could lead to a better understanding of non-perturbative QCD. Furthermore, modeling and subtracting of the DPS yield can provide input to single parton scattering (SPS) quarkonium production models. Quarkonium production contributes to backgrounds in some new physics searches.

An integrated luminosity of 11.4 fb$^{-1}$ of collision data is used. The prompt–prompt mesons accepted may be produced directly or through feed-down from $\psi(2S)$ or $\chi_c$ decays. Selected events satisfy a dimuon trigger requirement. The offline selection requires that events have at least three identified muons. In the reconstruction step, the distance between the two $J/\psi$ decay vertices along the beam direction, $|d_z|$, is determined. For each $J/\psi$ candidate, the signed transverse decay length, $L_{xy}$, is determined. The differential cross sections are measured in two regions based on rapidity $|y|$ of the sub-leading $J/\psi$: the central region ($|y| < 1.05$) and the forward region ($1.05 \leq |y| < 2.1$). The signal extraction procedure begins when each event is weighted by the inverse of the trigger, reconstruction, and selection efficiencies and the kinematic acceptance. An inclusive di-$J/\psi$ signal is obtained, and from this the prompt–prompt signal is obtained by ex-

amination of the $L_{xy}$ distribution, noting that the signal distribution will be modeled by a multi-Gaussian resolution function, while the non-prompt background can be modeled with a single-sided exponential function with decay constant $\tau$. Pile-up background is subtracted by applying the condition $|d_z| > 1.2$ mm. To determine the DPS fraction, a data-driven DPS template is constructed by combining $J/\psi$ mesons from different random events in the di-$J/\psi$ sample. The template for the SPS component is obtained by subtracting the DPS template from the $\Delta y$ *versus* $\Delta\phi$ distribution of the background-subtracted data. From these templates, DPS and SPS weights are computed, and with these applied (as well as the prompt–prompt weight) to every event, the prompt–prompt SPS and DPS signals are extracted as well as the fraction $f_{\mathrm{DPS}}$. Then for this fixed $f_{\mathrm{DPS}}$, the weighted data distributions are compared to the sum of the leading order (LO) DPS and the next-to-leading order color singlet without loops (NLO*) SPS predicted distributions. The effective cross section is calculated and compared to the measured values.

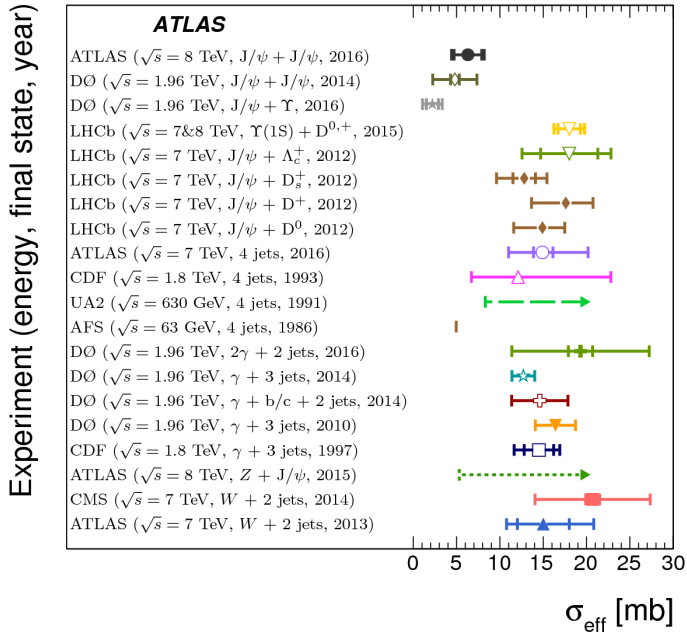


Fig. 2. The effective cross section of DPS from different energies and final states measured by the AFS, UA2, CDF, DØ, CMS, LHCb, and ATLAS experiments. The inner error bars represent the statistical uncertainties and the outer error bars represent the sum in quadrature of the statistical and systematic uncertainties. Dashed arrows indicate lower limits and the vertical line represents the AFS measurement published without uncertainties.

The prompt–prompt cross section $\sigma(pp \to J/\psi J/\psi + X)$ in the two rapidity bins of the sub-leading $J/\psi$ meson is found to be $82.2 \pm 8.3(\text{stat.}) \pm 6.3(\text{syst.}) \pm 0.9(\text{BF}) \pm 1.6(\text{lumi.})$ pb, for $|y| < 1.05$; and $78.3 \pm 9.2(\text{stat.}) \pm 6.6(\text{syst.}) \pm 0.9(\text{BF}) \pm 1.5(\text{lumi.})$ pb, for $1.05 \leq |y| < 2.1$. The cross sections are reported under the assumption of unpolarized $J/\psi$ mesons. The shape of the data-driven DPS distribution approximately agrees with the shape of the DPS predictions. There is however disagreement between the total data distribution and the total theory prediction at large $\Delta y$ and large invariant mass, and in the low-$p_{\text{T}}$ region. Possible explanations for the difference at large $\Delta y$ and invariant mass might be related to the intrinsic parton transverse momentum or a contribution via feed-down from a color-singlet $\psi(2S)$ meson. For single parton scattering, the results are characterized by distributions wider than the next-to-leading order predictions. The fraction $f_{\text{DPS}}$ is measured to be $(9.2 \pm 2.1(\text{stat.}) \pm 0.5(\text{syst.}))\%$, consistent with model predictions. A theoretical model based on LO DPS plus NLO* describes the data well. The effective cross section for prompt $J/\psi$ meson pair production is measured to be $\sigma_{\text{eff}} = 6.3 \pm 1.6(\text{stat.}) \pm 1.0(\text{syst.}) \pm 0.1(\text{BF}) \pm 0.1(\text{lumi.})$ mb. The effective cross section measured in this analysis is compared to measurements from other experiments and processes in Fig. 2.

## 4. $\psi(2S) \to J/\psi\pi^+\pi^-$ and $X(3872) \to J/\psi\pi^+\pi^-$ production

A measurement [4] of the differential cross sections for the production of $\psi(2S)$ and $X(3872)$ states in the decay channel $J/\psi\pi^+\pi^-$ is performed. The prompt and non-prompt production of each is studied separately, permitting examination of direct production and production via feed-down from one or more heavy hadrons. The production mechanism of the dipion final state is also examined.

Events used in this analysis are triggered by a pair of muons successfully fitted to a common vertex. The data sample corresponds to an integrated luminosity of 11.4 fb$^{-1}$. Events with two oppositely charged muon candidates are reconstructed and kept if the invariant mass of the dimuon system is consistent with that of a $J/\psi$ meson. The dimuon invariant mass is then constrained to the $J/\psi$ mass, and a four-track vertex fit is performed on the two muon tracks and pairs of non-muon tracks assigned pion masses. The invariant mass distribution of the $J/\psi\pi^+\pi^-$ candidates selected for further analysis is presented in Fig. 3.

The production cross sections are measured in five bins of $J/\psi\pi^+\pi^-$ transverse momentum. In order to separate prompt from non-prompt production, the data sample in each $p_{\text{T}}$ bin is further divided into intervals of pseudo-proper lifetime. To determine the yields of the signals, the distributions are fitted in each lifetime interval to a function that includes the signal forms, the background, threshold mass, and normalization terms, and the

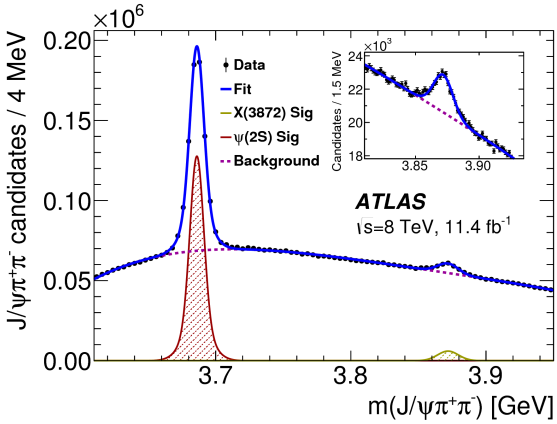


Fig. 3. The invariant mass of the selected $J/\psi\pi^+\pi^-$ candidates collected over the full $p_{\mathrm{T}}$ range 10–70 GeV and the rapidity range $|y| < 0.75$ after selection requirements. The curve shows the results of the fit using double-Gaussian functions for the $\psi(2S)$ and $X(3872)$ peaks and a fourth-order polynomial for the background. The $X(3872)$ mass range is highlighted in the inset.

signal yields for both species are extracted. With these yields $Y^i$ (where $i = \psi(2S)$ or $X(3872)$) determined in each $p_{\mathrm{T}}$ bin, the double differential cross sections times the product of the relevant branching fractions are calculated

$$B\left(i \to J/\psi\pi^+\pi^-\right) B\left(J/\psi \to \mu^+\mu^-\right) \frac{\mathrm{d}^2\sigma(i)}{\mathrm{d}p_{\mathrm{T}}\Delta y} = \frac{Y^i}{\Delta p_{\mathrm{T}} \Delta y \int L\mathrm{d}t}\,.$$

Initially, the non-prompt components of the signal distribution are described by a single one-sided exponential smeared with the resolution function, with an effective lifetime $\tau_{\mathrm{eff}}$. While for the $\psi(2S)$ the fitted values of $\tau_{\mathrm{eff}}$ are measured to be the same in all $p_{\mathrm{T}}$ bins, the signal from $X(3872)$ at low $p_{\mathrm{T}}$ tends to have shorter lifetimes, possibly hinting at a different production mechanism at low $p_{\mathrm{T}}$. An alternative model allows for two non-prompt contributions with distinctly different effective lifetimes. Any long-lived part of the non-prompt contribution is assumed to originate from $B^{\pm}, B^0$, and $B_s$ mesons and from $b$-baryons, while any short-lived part would be due to the contribution of $B_c^{\pm}$ mesons. The short-lived contributions to non-prompt $\psi(2S)$ production are found to be not significant. The fraction of non-prompt $X(3872)$ from short-lived sources, integrated over the range $p_{\mathrm{T}} > 10$ GeV, gives

$$\frac{\sigma(pp \to B_c)B(B_c \to X(3872))}{\sigma(pp \to \text{non-prompt } X(3872))} = (25 \pm 13(\text{stat.}) \pm 2(\text{syst.}) \pm 5(\text{spin}))\%\,.$$

The measured ratio of long-lived $X(3872)$ to long-lived $\psi(2S)$ is extracted with a Monte Carlo template to obtain

$$\frac{B(B \to X(3872) + \text{any})B\,(X(3872) \to J/\psi\pi^+\pi^-)}{B(B \to \psi(2S) + \text{any})B\,(\psi(2S) \to J/\psi\pi^+\pi^-)} = (3.57 \pm 0.33(\text{stat.}) \pm 0.11(\text{syst.})) \times 10^{-2}\,.$$

This ratio is smaller than the value $0.18 \pm 0.08$ obtained by using an estimate for the numerator obtained from the Tevatron data, and the world average values for the branching fractions in the denominator.

The measured differential cross section times the product of the relevant branching fractions for prompt production of $\psi(2S)$ is described fairly well by the NLO NRQCD model with long-distance matrix elements determined from the Tevatron data, below the highest $p_{\mathrm{T}}$ values. The $k_{\mathrm{T}}$ factorization model including color-octet contributions tuned to 7 TeV CMS data, and color singlet production, describes the data well but underestimates them at high $p_{\mathrm{T}}$ values. The NNLO* Color Singlet Model predictions agree with the data at low $p_{\mathrm{T}}$. The differential cross section for non-prompt $\psi(2S)$ is described well by the FONLL calculation over the whole range of transverse momenta. The differential cross section for prompt production of $X(3872)$ is described within theoretical uncertainty by the prediction of the NRQCD model which considers $X(3872)$ to be a mixed $\chi_{c1}(2P)$–$D^0\bar{D}^{*0}$ state. The measured differential cross section for non-prompt production of $X(3872)$ is compared to a calculation based on the FONLL model prediction for $\psi(2S)$. That calculation overestimates the data by a factor increasing with $p_{\mathrm{T}}$ from about 4 to about 8. Using normalized differential decay width distributions in bins of $m_{\pi\pi}$, pion production through the $\rho^0$ meson is found to be favored in the case of both the $\psi(2S)$ and the $X(3872)$ decays.

## 5. An angular analysis of $B_d^0 \to K^*\mu^+\mu^-$ decays

An angular analysis of the $B_d^0 \to K^*(892)\mu^+\mu^-$ is presented [5], where $K^*(892) \to K^+\pi^-$. Measurements of the $K^*$ longitudinal polarization fraction and a set of angular parameters obtained for the decay are compared with theoretical predictions. The observables can be sensitive to different types of new physics introduced as flavor-changing neutral current (FCNC) processes at tree or loop level. The angular variables used to describe the decay are (see Fig. 4):

— the angle between the $K^+$ and the direction opposite to the $B_d^0$ in the $K^*$ center-of-mass frame ($\theta_K$);

— the angle between the $\mu^+$ and the direction opposite to the $B_d^0$ in the dimuon center-of-mass frame ($\theta_L$); and

— the angle between the two decay planes formed by the $K\pi$ and the dimuon systems in the $B_d^0$ rest frame ($\phi$).

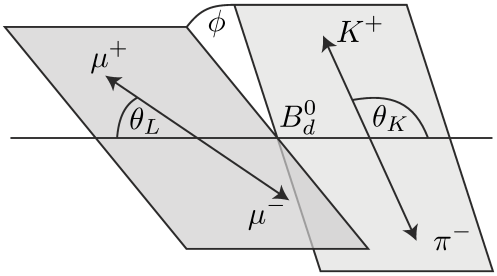


Fig. 4. An illustration of the $B_d^0 \to K^*\mu^+\mu^-$ decay showing the angles $\theta_K$, $\theta_L$, and $\phi$ defined in the text.

A form to express the angular differential decay rate is

$$\begin{aligned}\frac{1}{\mathrm{d}\Gamma/\mathrm{d}q^2}\frac{\mathrm{d}^4\Gamma}{\mathrm{d}\cos\theta_L\mathrm{d}\cos\theta_K\mathrm{d}\phi\mathrm{d}q^2} &= \frac{9}{32\pi}\Bigg[\frac{3(1-F_L)}{4}\sin^2\theta_K + F_L\cos^2\theta_K \\ &+\frac{1-F_L}{4}\sin^2\theta_K\cos 2\theta_L \\ &-F_L\cos^2\theta_K\cos\theta_L \\ &+S_3\sin^2\theta_K\sin^2\theta_L\cos 2\phi \\ &+S_4\sin 2\theta_K\sin 2\theta_L\cos\phi \\ &+S_5\sin 2\theta_K\sin\theta_L\cos\phi \\ &+S_6\sin^2\theta_K\cos\theta_L \\ &+S_7\sin 2\theta_K\sin\theta_L\sin\phi \\ &+S_8\sin 2\theta_K\sin 2\theta_L\sin\phi \\ &+S_9\sin^2\theta_K\sin^2\theta_L\sin 2\phi\Bigg].\end{aligned}$$

The familiar forward–backward asymmetry is given by $A_{\mathrm{FB}} = 3S_6/4$. The $S_i$ parameters depend on hadronic form factors which have significant uncertainties at leading order. It is possible to reduce the theoretical uncertainty on the parameters extracted from data by transforming the $S_i$ using ratios constructed to cancel form factor uncertainties at leading order. These ratios are given as

$$\begin{aligned}P_1 &= \frac{2S_3}{1-F_L}, \\ P_2 &= \frac{2}{3}\frac{A_{\mathrm{FB}}}{1-F_L},\end{aligned}$$

$$P_3 = -\frac{S_9}{1-F_L},$$
$$P'_{i=4,5,6,8} = \frac{S_{j=4,5,7,8}}{\sqrt{F_L(1-F_L)}}.$$

All of these parameters depend on the invariant mass squared of the dilepton system, $q^2$. The data are analyzed in $q^2$ bins to obtain an average value for a given parameter in that bin. Measurements of these quantities can be used as inputs to global fits used to determine the values of Wilson coefficients and search for new physics.

The events used in this analysis satisfy a trigger that requires one, two, or more muons. The study is based on 20.3 fb$^{-1}$ of integrated luminosity. Muon tracks are formed offline, and pairs of oppositely charged muons are required to originate from a common vertex. Candidate $K^*$ mesons are formed using pairs of oppositely charged kaon and pion candidates. As the ATLAS detector does not have a dedicated charged particle identification system, candidates are reconstructed to satisfy both possible $K\pi$ hypotheses and the selection relies on the kinematics of the reconstructed $K^*$ meson to determine which of the two tracks corresponds to the kaon. $B$ candidates are reconstructed from a $K^*$ candidate and a pair of oppositely charged muons. Extended unbinned maximum likelihood fits of the angular distributions in the data are compared to a model using a Gaussian signal function and other parameters taken from control region samples.

With the exception of the $P'_4$ and $P'_5$ measurements in $q^2 \in [4.0, 6.0]$ GeV$^2$ and $P'_8$ in $q^2 \in [2.0, 4.0]$ GeV$^2$, there is a good agreement between theory and measurement. The deviation, relative to the Standard Model calculations, observed for $P'_4(P'_5)$ is consistent with a deviation (Ref. [4] of the paper cited in [5]) reported by the LHCb Collaboration, and it is approximately 2.5(2.7) standard deviations from the calculation of DHMV (Ref. [14] of the paper cited in [5]). All measurements are found to be within three standard deviations of the range covered by the various predictions considered. Hence, including experimental and theoretical uncertainties, the measurements are found to be in accordance with the expectations of the Standard Model contributions to this decay.

## 6. Summary

ATLAS has presented four measurements using data recorded at $\sqrt{s} =$ 8 TeV at the LHC. All are compared to predictions by contemporary models.

— Differential cross sections for $b$-hadron pair production are measured to improve the theoretical description of quarkonium production and to facilitate background subtractions in new physics searches;

— Prompt $J/\psi$ pair production differential cross sections are measured to characterize double parton scattering as a probe of the gluon distribution of the proton, and to investigate correlations in the non-perturbative regime;

— Differential production cross sections for $\psi(2S)$ and $X(3872)$, both observed in decays to $J/\psi\pi^+\pi^-$, provide information about production mechanisms through examination of prompt and non-prompt signals; and

— An angular analysis of $B_d^0 \to K^*\mu^+\mu^-$ decays serves as a potential probe of new physics contributions through penguin diagrams.

## REFERENCES

[1] ATLAS Collaboration, *JINST* **3**, S08003 (2008).
[2] ATLAS Collaboration, *J. High Energy Phys.* **1711**, 062 (2017).
[3] ATLAS Collaboration, *Eur. Phys. J. C* **77**, 76 (2017).
[4] ATLAS Collaboration, *J. High Energy Phys.* **1701**, 117 (2017).
[5] ATLAS Collaboration, Angular Analysis of $B_d^0 \to K^*\mu^+\mu^-$ Decays in $pp$ Collisions at $\sqrt{s} = 8$ TeV with the ATLAS Detector, ATLAS-CONF-2017-023, `https://cds.cern.ch/record/2258146`